https://doi.org/10.5194/wes-2026-194
Preprint. Discussion started: 6 November 2026
© Author(s) 2026. CC BY 4.0 License.

eawe european academy of wind energy
Open Access WIND ENERGY SCIENCE DISCUSSIONS

Probabilistic Anchor Design for Floating Offshore Wind Turbines using Whole-Life Geotechnical Modelling

Ed Mackay[1], Ajit C. Pillai[1], and Katherine Kwa[2]

[1]University of Exeter, Penryn Campus, TR10 9FE, UK
[2]University of Southampton, Boldrewood Innovation Campus, Southampton SO16 7QF, UK

Correspondence: Ed Mackay (e.mackay@exeter.ac.uk)

Abstract. Floating offshore wind turbines require anchoring systems capable of sustaining variable cyclic loads over their operational lifetime, which may induce changes in seabed strength and anchor capacity. Conventional anchor design approaches are based on the conservative assumption that the largest applied load over the design lifetime occurs when the seabed soil is at its weakest state. To address this conservatism, this paper presents a probabilistic design framework for floating and deepwater offshore wind anchors utilising whole-life geotechnical modelling. This approach accounts for both the reduction in seabed strength due to cyclic loading and the potential increases in strength resulting from consolidation. The proposed framework involves generating time series of metocean conditions, simulating whole-life anchor loading via a probabilistic surrogate model, calculating soil damage accumulation and consolidation, and estimating the risk of failure over multiple lifetimes. The methodology is demonstrated using a case study of a 15 MW floating offshore wind turbine located in the Scottish North Sea. The results show that seabed strength initially decreases rapidly under cyclic loading and subsequently recovers through consolidation, with relatively little variation (less than 3.5%) in the strength evolution between different metocean realisations. Accounting for whole-life seabed hardening reduces the required anchor area by 6–8% for the baseline load distribution. However, sensitivity analysis shows that substantially larger reductions, of up to 27%, are possible when the distribution of extreme loads has greater separation from frequently occurring loads. The results therefore indicate that the benefit of whole-life geotechnical design is governed not only by the magnitude and rate of seabed strength recovery, but also by the relationship between frequent operational loading and rare extreme loading.

1 Introduction

The extension of offshore wind into deeper waters creates increasing demand for mooring and anchoring systems that can be deployed economically at scale. Floating platforms, together with emerging moored support concepts, may require several seabed anchors per turbine. Their design therefore has consequences for both project cost and the practical delivery of large offshore wind developments. This study considers how the required dimensions of embedded plate anchors can be assessed whilst accounting for changes in the seabed properties over the deployment lifetime. Deeply embedded plate anchors are an efficient and versatile anchoring solution for floating offshore wind applications as they can be installed or embedded into soft seabeds in a number of ways, via drag embedment, free fall, screwing or via a suction anchor (Cerfontaine et al., 2023).

https://doi.org/10.5194/wes-2026-194
Preprint. Discussion started: 6 November 2026
© Author(s) 2026. CC BY 4.0 License.



eawe european academy of wind energy
Open Access WIND ENERGY SCIENCE DISCUSSIONS

For a deeply embedded plate anchor, failure is assumed to occur when the applied load exceeds the ultimate undrained capacity, Q_{ult}. This capacity represents the short-term resistance of the anchor under loading conditions for which the excess pore water pressures generated in the surrounding seabed do not have sufficient time to dissipate. The ultimate capacity is given by (DNV, 2021)

$$Q_{ult} = \frac{N_c A_p s_u}{\gamma_m}, \tag{1}$$

where A_p denotes the area of the anchor plate, s_u is the available shear strength of the surrounding soil, which may be approximated by its volume-averaged value around the anchor (Stanier and White, 2019), N_c is the bearing factor relating soil shear strength to anchor resistance,[1] and γ_m is a resistance factor.[2] Under cyclic loading conditions, the seabed strength s_u decreases as a result of a build up in excess pore water pressure and reduction in soil effective stress. Reduction in soil strength is typically captured by cyclic degradation 'SN' curves, which follow a similar damage accumulation concept used in fatigue assessment (Andersen and Lauritzen, 1988; Andersen et al., 2015; Verruijt, 1995; Bonjean et al., 2008; Randolph and Gourvenec, 2017; Tom et al., 2019; Laham et al., 2025b; Kwa et al., 2023a).

In traditional anchor design methods, only decreases in seabed strength, s_u, and corresponding reductions in anchor capacity, Q_{ult}, are considered. Current anchor design principles are based on the assumption that the largest load over the design lifetime, occurs at the time when the soil is at its weakest state (DNV, 2021). This conservative assumption results in correspondingly conservative designs. Such conservatism is undesirable for FOW and ODOW applications, where individual farms are anticipated to require the installation of hundreds of anchors.

In soft soils, there is also potential for recovery in seabed strength as a result of consolidation, where the build up of excess pore water pressure is dissipated. Whole-life geotechnical design methods account for both reduction and increases in seabed strength in response to loading and seabed consolidation, offering a promising route to more efficient anchor designs (Gourvenec, 2020, 2022; Zhang et al., 2022; Kwa et al., 2023a; Rui et al., 2024; Laham et al., 2025b). Gains in soil strength due to consolidation effects in response to cyclic loading have been measured in penetrometer tests (Hodder et al., 2013; O'Loughlin et al., 2020), direct simple shear element tests (Laham et al., 2021, 2025a), large scale laboratory tank tests and geotechnical centrifuge tests of pipelines (Smith and White, 2014), sliding foundations (Cocjin et al., 2014, 2017), anchors (Han et al., 2016; Zhou et al., 2020; Wang et al., 2023) and pile foundations (Lai et al., 2020; White et al., 2022). These studies highlight the potential of design approaches that quantify changes in seabed strength and anchor capacity, to allow for more accurate assessment of anchor failure risks over the design lifetime. Such an advance would parallel developments in structural reliability analysis where time-dependent changes are recognised and quantified within models (Bai et al., 2016).

Assessing this history-dependent behaviour requires loading information throughout the intended service period, not only estimates of the largest expected tension. A direct calculation using an hour-long dynamic simulation for every hourly state in a 20-year sequence would entail approximately 175,000 response simulations for a single lifetime. Using a surrogate model

[1] For a rough plate embedded sufficiently deeply that the failure mechanism does not extend to the seabed surface, the theoretical bearing factor is $N_c = 13.11$ (Martin and Randolph, 2001).

[2] To isolate the influence of changes in seabed strength, we take $\gamma_m = 1$ throughout this study.

https://doi.org/10.5194/wes-2026-194
Preprint. Discussion started: 6 November 2026
© Author(s) 2026. CC BY 4.0 License.



eawe european academy of wind energy
Open Access WIND ENERGY SCIENCE DISCUSSIONS

can significantly reduce the computational burden, and reduce the number of dynamic simulations required to estimate the responses over all environmental conditions over the deployment lifetime (Jiang et al., 2020; Samadian et al., 2025).

In this work, we present a probabilistic design framework for anchors, using a whole-life geotechnical modelling approach. The approach is applicable to both floating offshore wind turbines (FOWTs) and moored hybrid structures. In the design framework, we assume that the design of the turbine, support structure, and mooring are fixed, and we are interested in optimising the anchor design. The probabilistic design framework involves the following steps:

1. Generation of many realisations of metocean conditions over a deployment lifetime;
2. Simulation of whole-life anchor loading from a probabilistic surrogate model;
3. Calculation of soil damage accumulation and consolidation; and
4. Estimation of risk of failure over many possible lifetimes.

We demonstrate the method using a case study for a 15 MW FOWT at a site in the Scottish North Sea. The case study makes use of a probabilistic surrogate model for anchor loading for this turbine and location, developed in previous work (Mackay et al., 2026a, b). Similarly, the calculation of soil damage accumulation and consolidation is based on the method presented by Kwa et al. (2023a). The purpose of this work is to bring together these aspects in a combined framework, so that the effects of soil consolidation on anchor designs can be assessed. We compare the optimised anchor design using the whole-life approach to a design based on a calculation which only accounts for loss of soil strength and no hardening effects, akin to design methods recommended in current standards.

The paper is organised as follows. Section 2 presents an overview of the probabilistic design framework implemented in this work. Section 3 describes the soil and metocean conditions at the site used for the case study, as well as the turbine, support structure and moorings. The components of the probabilistic design framework are described in detail in Section 4. The results of the case study are presented in Section 5. Finally, conclusions are presented in Section 6.

2 Probabilistic design framework overview

The probabilistic design framework proposed in this work is intended to quantify the risk of anchor failure over the design lifetime, by accounting for through-life changes in seabed strength and anchor capacity as a result of anchor loading histories. The probabilistic design framework could be expanded to include random variability or uncertainty for the in-situ seabed parameters, which can also affect anchor resistance (Cai et al., 2022; Mentani et al., 2025). However, this was not explored in this study. In order to understand the rationale for our proposed method, we start by presenting an overview of an 'explicit' probabilistic design framework in Section 2.1, and explain the difficulties in implementing such a method. Section 2.2 then describes how our proposed approach addresses these challenges.

https://doi.org/10.5194/wes-2026-194
Preprint. Discussion started: 6 November 2026
© Author(s) 2026. CC BY 4.0 License.

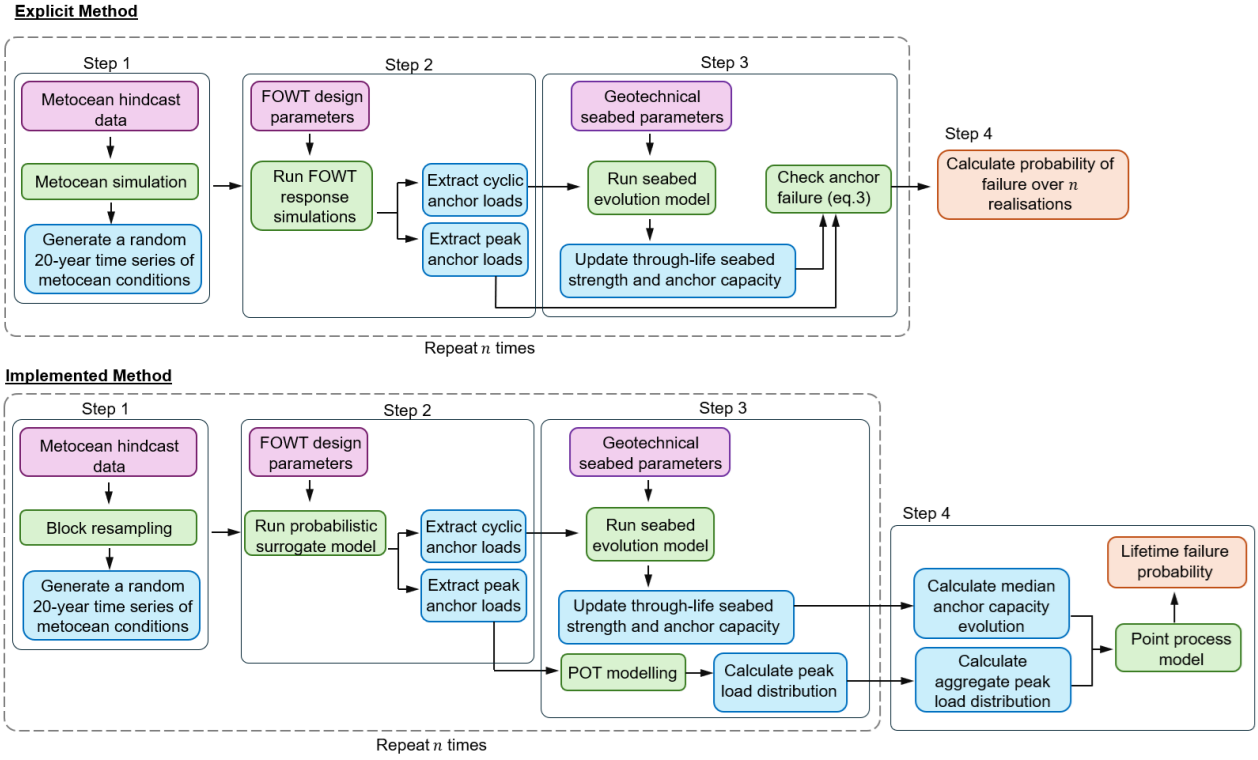


Figure 1. Overview of probabilistic anchor design framework. Top: Explicit method with fully-random metocean simulation. Bottom: Method implemented in this work, where metocean data is resampled. In this case, metocean conditions are never more extreme than observed in the input data, so additional steps must be taken to extrapolate the anchor loads.

2.1 Explicit method

A flow diagram of the steps involved in the explicit method is shown in Figure 1. The method involves simulating many possible lifetimes of the FOWT (of the order of 20 years), and calculating the proportion of lifetimes in which the anchor fails. The first step in the method is to generate a random time series of metocean conditions, with statistical properties based on a historic metocean dataset. Simulation of random multivariate time series, which accurately replicate both the multivariate distribution and temporal correlation structure of an observed dataset, is a difficult challenge for which no fully-general solution has been proposed. This is especially true in relation to extreme conditions (see e.g. Tendijck et al., 2024; Clarindo et al., 2026), which are important with regard to anchor loading.

The second step is to simulate the FOWT and mooring response to each environmental condition in the random metocean time series. As discussed in the introduction, conducting time domain simulations for each 1-hour period of a 20-year time series, is not computationally feasible for most projects. If this is repeated over N possible lifetimes of metocean conditions then the computational requirement is N times higher.

https://doi.org/10.5194/wes-2026-194
Preprint. Discussion started: 6 November 2026
© Author(s) 2026. CC BY 4.0 License.



eawe european academy of wind energy
Open Access WIND ENERGY SCIENCE DISCUSSIONS

The next step is to calculate the changes in seabed strength in response to the cyclic loading over the lifetime. This is then used to create a time series anchor capacity $Q_{ult}(t)$ over the design lifetime, which is compared to the lifetime of anchor loads $Q(t)$ to check if the anchor has failed. We define the mobilised anchor capacity at any given time t, as the ratio of the load to capacity:

$$Q_{mob}(t) = \frac{Q(t)}{Q_{ult}(t)}. \tag{2}$$

The anchor is considered to have failed if

$$\max_{t\in[0,T]} Q_{mob}(t) > 1, \tag{3}$$

where T is the design lifetime.

2.2 Method implemented in this work

The two key challenges with implementing the explicit method, outlined above, are simulating realistic metocean time series and calculating load responses to each metocean condition. As noted in the introduction, to address the computational challenge of simulating responses over each random lifetime of metocean conditions, we use a probabilistic surrogate model. For the metocean simulation, we implement a simple scheme using a block resampling approach. This produces a random sequencing of the observed metocean conditions, whilst preserving the short-term temporal correlation structure within blocks. This method is simple to implement, but has the drawback that the resampled time series are never more extreme than in the hindcast dataset. Since the soil evolution is driven by cyclic rather than extreme loading, we demonstrate below that this gives a reasonable estimate of the changes in seabed strength over the deployment lifetime. In fact, there is very little variation in the evolution of seabed strength over different random realisations of metocean conditions. We show that this enables a single median anchor capacity evolution to be used in design calculations.

To address the limitations of the block resampling approach, we extrapolate the peak loads for each realisation, using a peaks-over-threshold (POT) method. This is then used to form an aggregated peak load distribution over possible lifetimes, which is then combined with the median anchor capacity evolution to estimate the probability of failure. The justifications and details of each calculation step are provided in Section 4. First, we outline the parameters of the case study used to illustrate the design framework.

3 Case study parameters

3.1 Location

The case study presented in this work is for a site in the Scottish North Sea ($58.20°$ N, $0.60°$ W), at a location representative of areas being developed for FOW farms. The location is illustrated in Figure 2, together with the bathymetry in the region. The site selected has a water depth of 100 m, which is characteristic of the FOWT farms currently under development in the UK[3].

[3]See: https://www.crownestatescotland.com/scotlands-property/offshore-wind/scotwind-leasing-round

https://doi.org/10.5194/wes-2026-194
Preprint. Discussion started: 6 November 2026
© Author(s) 2026. CC BY 4.0 License.

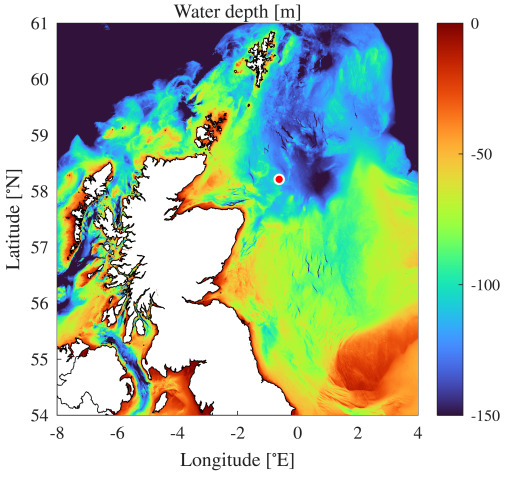


Figure 2. Location of site used in case study (red dot) off the east coast of Scotland, with a water depth of 100 m.

3.2 Turbine and support structure

We consider the IEA 15 MW reference turbine (Gaertner et al., 2020) installed on the VolturnUS-S semi-submersible platform (Allen et al., 2020). We adopt the same turbine–mooring configuration used to develop the load surrogates in Mackay et al. (2026a, b), so that the present study isolates the consequences of the anchor design methodology rather than changing the floating system. The rotor diameter is 240 m and the hub elevation is 150 m above sea level. The turbine operates for wind speeds between 3 and 25 m/s, with rated wind speed 10.59 m/s.

Station keeping is provided by three semi-taut mooring lines in 100 m water depth, with an arrangement adapted from Kwa et al. (2023b). Each line contains a 122.75 m polyester segment of 266 mm diameter, connected to 10 m chain sections at each end; the lower section is 185 mm R3 studless chain. In still water with no wind forcing, the tension at the seabed end of line 1 is 1888 kN. The calculated natural periods are 45.2 s for surge, 18.6 s for heave and 22.6 s for pitch. This arrangement is illustrated in Figure 3.

3.3 Metocean conditions

Metocean data was taken from the UK Met Office wave-model archive at the study location, using 3-hourly records for 1980–2023 on a 1.5 km grid (UK Met Office, 2025). The variables passed to the load surrogate are significant wave height, H_s, peak wave period, T_p, and the one-hour mean wind speed at turbine hub height, U_{hub}. The archived 10 m wind speed is adjusted to 150 m using a power-law profile with exponent 0.14, in accordance with the IEC 61400-3-1 IEC (2019). Because the reported peak periods contain discretisation artefacts, peak period is instead estimated from the spectral mean period, $T_m = m_0/m_1$, where m_j is the j-th moment of the wave frequency spectrum. For the JONSWAP spectrum used in the re-

https://doi.org/10.5194/wes-2026-194
Preprint. Discussion started: 6 November 2026
© Author(s) 2026. CC BY 4.0 License.

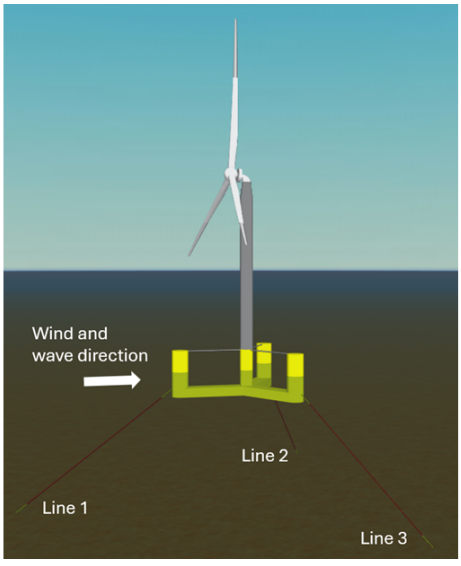


Figure 3. Rendering of the IEA 15 MW turbine on the Volturn-US platform with a semi-taut mooring.

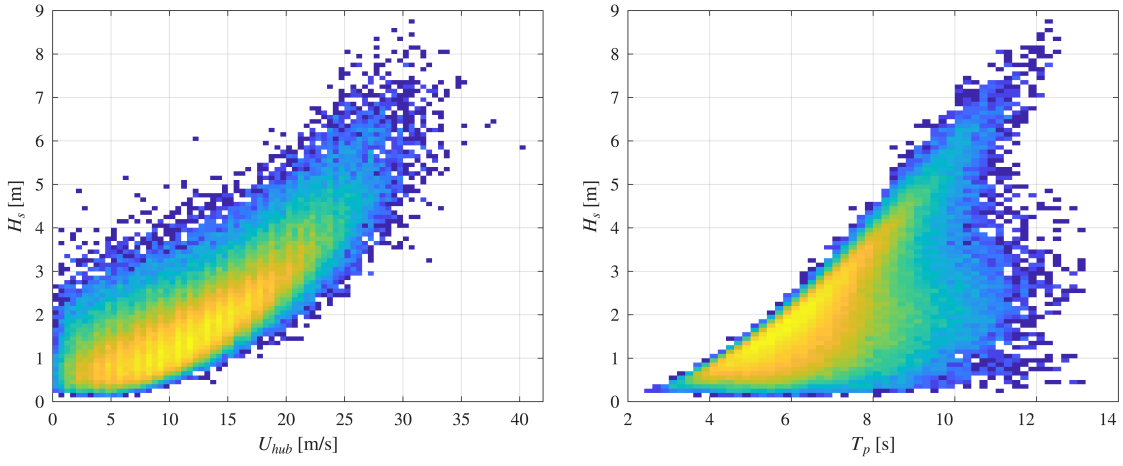


Figure 4. Empirical densities of wind and wave variables (blue = low density, yellow = high density).

sponse model (peak enhancement factor 3), we take $T_p = 1.2063T_m$. Figure 4 shows the empirical joint densities of the wind and wave variables.

https://doi.org/10.5194/wes-2026-194
Preprint. Discussion started: 6 November 2026
© Author(s) 2026. CC BY 4.0 License.



eawe european academy of wind energy
Open Access WIND ENERGY SCIENCE DISCUSSIONS

3.4 Soil conditions

The seabed soil type at this case study's location is classified as a mixture of mud and sandy mud (Marine Scotland, 2013). Representative material parameters that are typical for these materials, which are similar to normally to lightly consolidated soft clays and silts, have been selected and are summarised in Table 1.

4 Model components

In this section we present an overview of each of the modelling steps in the probabilistic design framework, illustrated in Figure 1.

4.1 Soil evolution model

In this work, the effect of cyclic loading on seabed strength is modelled using the RSN-CSI approach described in Kwa et al. (2023a). This model was developed for assessing the whole-life behaviour of an embedded plate anchor in soft clay during the application of variable cyclic amplitudes throughout operational lifetimes. The model has two steps. In the first, 'RSN' step, the effect of cyclic loads within a sea state is quantified in terms of a damage parameter, D. In the second, 'CSI' step, the effects of consolidation and dissipation of pore pressure are calculated in terms of the damage, D, and a hardening parameter, H. The damage and hardening parameters are then used to quantify the change in seabed strength, s_u. These two steps are applied at each time step (of the order of 1 to 3 hours) over the proposed lifetime of the structure. We give a short description of each step below. Throughout this section we use the following notation. Let $t_1, , \ldots, t_K$ be the times corresponding to environmental conditions $\boldsymbol{x}_1, \ldots, \boldsymbol{x}_K$, damage $D_1, \ldots, D_K$ and hardening $H_1, \ldots, H_K$. The seabed strength and anchor ultimate capacity at time t_i are denoted $s_u(t_i)$ and $Q_{ult}(t_i)$, respectively.

4.1.1 RSN model

The 'RSN' part of the macro model[4] is used to calculate the accumulation of damage, D, from a time series of random cyclic loads over a short period, of the order of 1 to 3 hours. The damage takes a value in the range $0 \leq D \leq 1$, with the maximum value $D = 1$ corresponding to a loss in soil effective stress from excess pore water pressure build up from cyclic loading. However, when $D = 1$ the anchor still has some capacity, as the surrounding seabed strength, s_u, decreases to a minimum residual value, $s_{u,min}$ (see Section 4.1.2).

The damage accumulated over a sea state is calculated in terms of rainflow counts of load cycles applied to the anchor (ASTM International, 2023). For the time series of mooring line tension at the anchor point, from the simulation in sea state $\boldsymbol{x}_i$, a rainflow counting algorithm is used to define a sequence of m_i equivalent load cycles $(r_{i,1}, s_{i,1}, n_{i,1}), \ldots, (r_{i,m_i}, s_{i,m_i}, n_{i,m_i})$, where $r_{i,j}$ is the mean tension of cycle j, $s_{i,j}$ is the cycle amplitude, and $n_{i,j} = 0.5$ or 1 according to whether it is a half cycle or full cycle. The cycle means and amplitudes are normalised by the current anchor capacity as $\tilde{r}_{i,j} = r_{i,j}/Q_{ult}(t_i)$ and

[4] 'RSN' refers to the variables output by the rainflow counting algorithm, discussed below.

https://doi.org/10.5194/wes-2026-194
Preprint. Discussion started: 6 November 2026
© Author(s) 2026. CC BY 4.0 License.



eawe european academy of wind energy
Open Access WIND ENERGY SCIENCE DISCUSSIONS

$\tilde{s}_{i,j} = s_{i,j}/Q_{ult}(t_i)$. In the original method proposed by Kwa et al. (2023a), the ordering of load cycles affects the accumulated damage. However, for the particular application considered here, there is relatively little variation in the values of r_j over a one-hour sea state, and it was found that it made negligible difference to the accumulated damage to replace the random sequence $r_1, \ldots, r_m$ by the mean value over the response simulation, $\bar{r}_i = m_i^{-1} \sum_{j=1}^{m_i} \tilde{r}_{i,j}$ (see Mackay et al., 2026b, for details). In this case, the ordering of the cycles does not influence the accumulated damage, and the damage in sea state $\boldsymbol{x}_i$ can be calculated as

$$D_i = k_1(1+\bar{r}_i)^{k_5}\left(1-\exp\left(-b_{i-1}-k_2\sum_{j=1}^{m_i} n_{i,j}(\tilde{s}_{i,j}-k_4)_+^{k_3}\right)\right), \tag{4}$$

where $k_1, \ldots, k_5$ are constants describing the soil properties, $(x)_+ = \max(x, 0)$, and b_{i-1} describes the contribution from the damage accumulated up to sea state $i-1$, renormalised to mean tension $\bar{r}_i$, given by

$$b_{i-1} = -\log\left(1-\frac{D_{i-1}}{k_1(1+\bar{r}_i)^{k_5}}\right). \tag{5}$$

If the damage given by (4) is greater than 1, then we set $D_i = 1$. Throughout this work we assume that $D_0 = 0$ and hence $b_0 = 0$.

In the present work, the RSN model parameters have been calibrated to the damage contours for normally to lightly consolidated clays, similar to those presented in Andersen and Lauritzen (1988); Andersen et al. (2015), and are set as $(k_1, k_2, k_3, k_4, k_5) = (1, 22.58, 4, 0.001, 1)$. These parameters can be calibrated for other materials via cyclic element direct simple shear laboratory tests as described in Andersen et al. (2015).

4.1.2 CSI model

The 'CSI' part of the model is a soil mechanics 'Critical-State-Inspired' model, based on White et al. (2022), for calculating the combined effects of damage and consolidation on changes in soil strength, s_u. In the CSI model, the seabed strength s_u at time t_i depends on the hardening H_i and damage D_i, and is given by

$$\frac{s_u(t_i)}{s_{u0}} = \left(1+\frac{H_i}{\lambda_*}\right)\left(1-D_i\frac{(S_{t0}-1)(1-H_i)^q}{1+(S_{t0}-1)(1-H_i)^q}\right), \tag{6}$$

where s_{u0} is the initial undrained strength, S_{t0} and q are parameters describing the soil sensitivity to hardening, and λ_* is a dimensionless compression index, which controls the maximum gain in soil strength. The ratio s_u/s_{u0} is governed by the limiting cases $D = 0$ and $D = 1$. When $D = 0$ we have $s_u/s_{u0} = s_{u,max} = 1 + H/\lambda_*$, and when $D = 1$ we have $s_u/s_{u0} = s_{u,min} = (1 + H/\lambda_*)/(1 + (S_{t0} - 1)(1 - H)^q)$. These bound the possible range of values that s_u/s_{u0} can take as a function of H, as illustrated in Figure 5. When $H = 0$ and $D = 1$, we have $s_u/s_{u0} = 1/S_{t0}$. Conversely, when $H = 1$ and $D = 0$, we have $s_u/s_{u0} = 1 + 1/\lambda_*$.

The increase in the soil damage due to cyclic loading is given by the RSN model. The damage also decays over time due to pore pressure dissipation, leading to consolidation. The rate of damage dissipation is given by

$$\left.\frac{dD}{dt}\right|_{t=t_i} = -k_{d2}\frac{c_v}{B^2}D_i^{\beta}, \tag{7}$$

https://doi.org/10.5194/wes-2026-194
Preprint. Discussion started: 6 November 2026
© Author(s) 2026. CC BY 4.0 License.



eawe european academy of wind energy
Open Access WIND ENERGY SCIENCE DISCUSSIONS

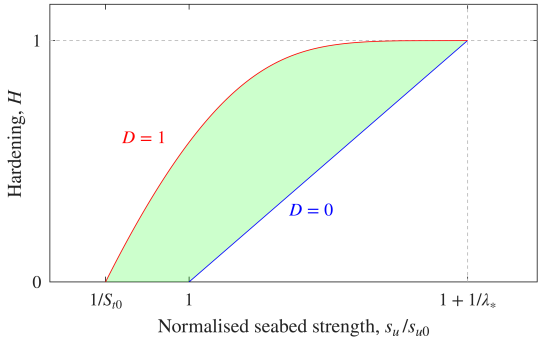


Figure 5. Bounds on range of values of normalised sea bed strength s_u/s_{u0} as a function of hardening parameter H. Only values in the green shaded area are possible, with bounds corresponding to limiting cases of damage $D = 0$ and $D = 1$.

where k_{d2} and β are dimensionless parameters, c_v is a coefficient of consolidation, and B is the anchor diameter. The rate of hardening is related to the rate of damage dissipation, and is given by

$$\left.\frac{dH}{dt}\right|_{t=t_i} = -k_{d2}\frac{c_v}{B^2}D_i^{\beta}\,\kappa_*(1-H_i)^{\gamma}, \tag{8}$$

where γ is a dimensionless parameter, and κ_* is a swelling index. Since pore pressure dissipation and soil consolidation effects are long-term processes, the unit of time in (7) and (8) is years. The maximum possible rate of hardening occurs when $D_i = 1$. If the rate of cyclic loading is such that $D_i = 1$ for $i = 1, ..., K$, then (8) with initial condition $H_0 = 0$ has the solution

$$H_i = 1 - \left(k_{d2}\frac{c_v}{B^2}\kappa_*(\gamma-1)t_i + 1\right)^{\frac{1}{1-\gamma}}. \tag{9}$$

This describes the maximum possible increase in hardening over time.

The CSI model parameter values for the seabed conditions at the case study location are listed in Table 1. These have been calibrated using centrifuge experiments that capture changes in soil strength and anchor capacity through application of whole-life loading on small scale plate anchors and a T-bar in samples of normally to lightly consolidated clays and silts (O'Loughlin et al., 2020; Zhou et al., 2020).

4.2 Surrogate response model

The whole-life calculations require two complementary descriptions of mooring tension: one for the peak load in each sea state, and another for the load cycles that drive changes in soil strength. Both are obtained from the previously developed probabilistic surrogate models (Mackay et al., 2026a, a). For each environmental state $X = (U_{hub}, H_s, T_p)$, the surrogate model returns parameters specifying the relevant conditional load distributions, from which stochastic response quantities can be sampled. This retains random variability between different wind and wave realisations even when their summary environmental conditions are the same.

https://doi.org/10.5194/wes-2026-194
Preprint. Discussion started: 6 November 2026
© Author(s) 2026. CC BY 4.0 License.



eawe european academy of wind energy
Open Access WIND ENERGY SCIENCE DISCUSSIONS

Table 1. CSI model parameters

Parameter	Symbol	Unit	Value(s)
Anchor diameter or width	B	m	variable
Soil strength gradient	k_{su}	kPa/m	2
Initial undrained seabed shear strength	s_{u0}	kPa	$2\,B\,k_{su}$
Initial sensitivity to hardening	S_{t0}	-	2.5
Coefficient of consolidation	c_v	m^2/year	2.5–10
Hardening index	q	-	0.3
Compression index	λ_*	-	0.5
Swelling index	κ_*	-	0.25
Dimensionless parameter for consolidation	k_{d2}	-	8
Dimensionless parameter for consolidation	β	-	1.1
Dimensionless parameter for hardening	γ	-	1.4

The surrogate construction, parameter estimation and validation are reported in the conference papers; the following sections give only the information needed to reproduce the whole-life design analysis.

4.2.1 Response simulations

The surrogate training data were generated by time-domain simulations in OrcaFlex 11.5 (Orcina Ltd, 2025). For each environmental input, an hour of response was retained after a 600 s initial ramp-up period. In the numerical model, the anchor connection at the mudline is represented as a fixed point with infinite stiffness. Consequently, the mooring line response is calculated without coupling to either the behaviour of the embedded line or the anchor-seabed interaction. The loads calculated at the mudline are assumed to be transferred directly to the anchor plate, without any reduction. Although load-reduction factors could be introduced to account for these effects (Rui et al., 2025), no such factors are applied in the present study. All simulations were run with turbulent winds and irregular waves, with a different random seed for the winds and waves for each simulation, to capture the stochastic variability.

The surrogate input space is limited to hub-height mean wind speed, significant wave height and peak wave period. Other environmental features were fixed in the original response simulations: water level was held constant, currents were excluded, wind shear followed the profile specified in Section 3.3, and the wind field used the IEC extreme-wind model with a Kaimal spectrum and 11% turbulence intensity. The waves followed a unidirectional JONSWAP spectrum with a peak enhancement factor of 3. Wind and waves were aligned with mooring line 1, which had been identified as the most heavily loaded line for the

https://doi.org/10.5194/wes-2026-194
Preprint. Discussion started: 6 November 2026
© Author(s) 2026. CC BY 4.0 License.



eawe european academy of wind energy
Open Access WIND ENERGY SCIENCE DISCUSSIONS

configurations examined. The intention was to represent a demanding loading direction while keeping the number of surrogate inputs tractable; it does not establish that all effects of the omitted environmental variability are conservative.

The simulation input conditions were selected to encompass the combinations recorded in the historical archive. The resulting datasets contain 1297 conditions used to train the surrogate and two additional groups of 350 conditions for validation and testing, respectively. Despite the relatively large number of simulations, this is still two orders of magnitude fewer than running simulations for each condition in the metocean dataset. Moreover, the number of simulations used here is similar to the number of load cases considered in a typical design analysis.

4.2.2 Surrogate fitting

Separate models were needed for power-producing and idling states because of the sharp change in turbine response at cut-out wind speed. The short-term peak-load surrogate follows Mackay et al. (2026a). It extracts local maxima from each simulated tension record, with peaks separated by a minimum of 10 s, estimates an environmentally varying threshold at the 70th percentile of the peaks, and models the excesses above that threshold using a generalised Pareto distribution. Neural-network functions relate the distribution parameters to the environmental inputs.

The cyclic-load surrogate follows Mackay et al. (2026b). Rainflow counting supplies the amplitudes and mean tensions of individual load cycles. The earlier study found that a single representative mean tension for each environmental state gave sufficiently accurate damage estimates, so only the load cycle amplitude distribution is modelled in the surrogate. Small cycles with negligible influence on calculated soil damage are separated from the larger cycles, and the latter are represented by a Weibull distribution.

Although the creation of a surrogate is a key step in enabling the whole-life geotechnical approach, we refer readers to Mackay et al. (2026a, b) for details of the model validation. In the present work, the same surrogate model is used to produce loads for both the reference design and whole-life design method. Therefore, any errors or uncertainties in the surrogate will affect both approaches. Another way to consider this is that we assume the surrogate is a perfect representation of the mooring loads and consider the effect of modelling varying seabed strength in isolation.

4.3 Metocean simulation model

The objective of the metocean simulation model is to create synthetic time series of metocean conditions that capture (1) the joint distribution of observed metocean variables, (2) the short-term temporal structure (i.e. evolution over the course of days to weeks), and (3) the seasonal variability. Correctly representing both the short-term and seasonal variability is important for assessing the effects of soil damage accumulation and consolidation. As discussed above, modelling both the joint distribution of multiple variables and their temporal evolution is a difficult problem. Resampling from observed conditions provides a simple solution to this. The key drawback of resampling is that the conditions in the resampled time series are never outside the range of the observations. This limitation is dealt with by response extrapolation, discussed below in Section 4.4.

To capture the short-term temporal dependence, we implemented a block resampling scheme (Künsch, 1989; Politis and Romano, 1994). Resampling blocks results in discontinuities at the boundaries between blocks. However, this is not important

https://doi.org/10.5194/wes-2026-194
Preprint. Discussion started: 6 November 2026
© Author(s) 2026. CC BY 4.0 License.



eawe european academy of wind energy
Open Access WIND ENERGY SCIENCE DISCUSSIONS

for our analysis. Block resampling captures both the joint distribution and short-term temporal structure. To capture the seasonal variability, we resample blocks as follows. For simplicity, we assume that the historic data covers a whole number of years, starting at January 1st on year y_1 and ending on December 31st on year y_m. Block start times in days are set as $t_i = i \times n_{block}$, $i = 0, 1, 2, ...$, where n_{block} is the number of days in the block. The day of the year used for the resampled block is set as $d_i = \mathrm{mod}\,(t_i + \delta_i, 365)$, where δ_i is a zero-mean normal variable with standard deviation σ_d. This random perturbation avoids resampling blocks with the same start times on each sample, and is based on the assumption that the climate is approximately stationary over short durations. We then resample blocks with start times (in years) $\tau_i = \gamma_i + d_i/365$, where γ_i is a random year in the set $\{y_1, ..., y_m\}$. If any of the start or end times of the blocks are outside the range of the metocean dataset, then we generate a new random pair (γ_i, d_i) for the block, and repeat until all resampled blocks lie within the historic range (typically this takes only one or two iterations).

In the present work we have set $n_{block} = 28$ days to capture any weather patterns that persist over periods longer than a few days, and $\sigma_d = 14$ days, so that $\approx 95\%$ of blocks have a start time within 28 days of the target start time. To assess the ability of this scheme to capture the seasonal variation in conditions, we compare the quantiles of each variable conditional on the day of year. For the hindcast data we calculate conditional quantiles at non-exceedance probabilities 0.1, 0.25, 0.5, 0.75 and 0.9, using a window of length 5 days. This is compared to the daily quantiles from 1000 resampled time series, each of length 20 years. The results are shown in Figure 6, and indicate that the resampling scheme provides a seasonal variation that is very close to the observed values, indicating the perturbation STD, σ_d, provides an appropriate level of smoothing.

4.4 Response extrapolation

By construction, the resampled metocean time series will never contain conditions outside the range in the historic data. Therefore, to estimate the failure probability due to peak loading, we cannot simply count the proportion of simulated lifetimes in which an anchor fails due to peak loads, as this will omit the probability that a more extreme environmental condition occurs than was previously observed. This problem arises naturally in extreme value analysis (EVA): commonly, we have a time series of observations and we wish to extrapolate to unobserved levels. If we had a single time series of peak loads, $Q(t)$, simulated from the surrogate, then extrapolation would be a standard EVA problem. The difference between the standard EVA problem and the current setup, is that we have multiple time series of $Q(t)$, each based on resampled metocean time series $\boldsymbol{x}(t)$, but with different random responses in each environmental condition. To account for this, we use the approach proposed by Mackay and Johanning (2018a, b).[5] The method proceeds as follows (details are discussed underneath):

1. Suppose we generate N time series of 3-hour peak loads, denoted $Q_1(t), \ldots, Q_N(t)$.
2. For time series $Q_i(t)$, we conduct a standard peaks-over-threshold (POT) analysis:
   (a) Extract peaks in the time series $P_{i,1}, P_{i,2}, \ldots$.
   (b) Select an appropriate threshold $u_{LT,i}$.

[5] Although originally developed for estimating return values of individual wave and crest heights, the method is directly applicable to estimating return values of any short-term response function (see Mackay et al., 2021).

https://doi.org/10.5194/wes-2026-194
Preprint. Discussion started: 6 November 2026
© Author(s) 2026. CC BY 4.0 License.

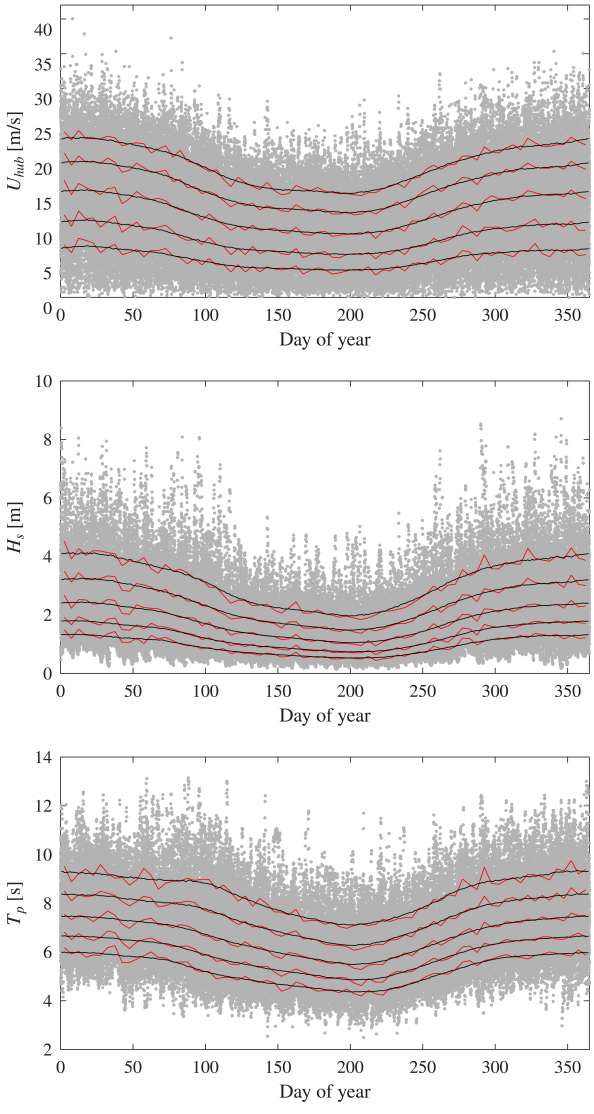


Figure 6. Seasonal variability in metocean variables. Historic data (grey dots) against day of year, with conditional quantiles at non-exceedance probabilities 0.1, 0.25, 0.5, 0.75 and 0.9 (red lines). Black lines show conditional quantiles calculated from 1000 resampled time series each of length 20 years.

https://doi.org/10.5194/wes-2026-194
Preprint. Discussion started: 6 November 2026
© Author(s) 2026. CC BY 4.0 License.

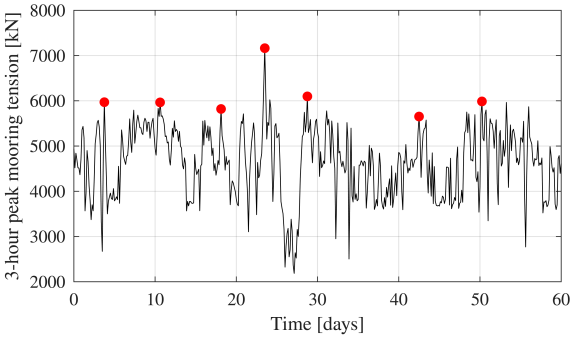


Figure 7. Example time series of 3-hour-maximum mooring tension (line), with peaks defined as local maxima within a moving window of ± 5 days (circles).

(c) Fit the generalised Pareto (GP) distribution to peaks exceeding the threshold, to yield shape and scale parameter estimates $(\xi_{LT,i}, \sigma_{LT,i})$.[6]

3. Finally, a peak in an arbitrary time series of loads is assumed to follow a GP distribution with the mean shape, scale and threshold over all simulated time series: $(\bar{\xi}_{LT}, \bar{\sigma}_{LT}, \bar{u}_{LT})$, where

$$\bar{\xi}_{LT} = \frac{1}{N}\sum_{i=1}^{N} \xi_{LT,i}, \quad \bar{\sigma}_{LT} = \frac{1}{N}\sum_{i=1}^{N} \sigma_{LT,i}, \quad \bar{u}_{LT} = \frac{1}{N}\sum_{i=1}^{N} u_{LT,i}.$$

In step 2(a) above, local peaks in the time series $Q_i(t)$ are defined as local maxima within a ± 5-day rolling window. An example of peaks identified within a short section of a time series is shown in Figure 7. In step 2(b), we define the threshold as the quantile of the peaks $P_{i,1}, P_{i,2}, \ldots$ at non-exceedance probability τ. The optimal value of τ is selected from inspection of diagnostic plots for a single time series, which check for the stability of the estimated shape parameter and a goodness-of-fit statistic (see Solari et al., 2017, for details). In step 2(c), the GP parameters are estimated using maximum likelihood estimation.

Exceedance probabilities of the peaks in the long-term mooring time series are shown in Figure 8, for 1000 realisations, together with the mean fitted GP distribution. The optimal non-exceedance probability for the threshold was found to be $\tau = 0.7$. Although there is some dispersion in the largest quantiles, the observed range of values agrees well with the theoretical sampling variability, based on a parametric bootstrap using the mean fitted GP parameters, indicating that the model is a good fit to the data.

[6]The subscript LT denotes long-term, to distinguish from the parameters of the GP distribution for short-term extreme responses, used in the probabilistic surrogate model.

https://doi.org/10.5194/wes-2026-194
Preprint. Discussion started: 6 November 2026
© Author(s) 2026. CC BY 4.0 License.

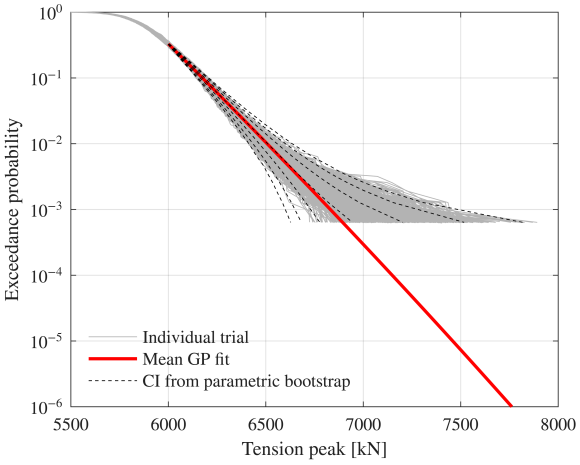


Figure 8. Exceedance probabilities of peaks in each of 1000 long-term time series of mooring tension, and mean fitted GP distribution. Dashed lines indicate quantiles from parametric bootstrap of the mean fitted GP distribution at non-exceedance probabilities 0.001, 0.01, 0.1, 0.5, 0.9, 0.99 and 0.999.

4.5 Failure probability calculation

The failure probability calculation is based on two assumptions. Firstly, we assume that the time evolution of $Q_{ult}(t)$ is deterministic and known. Secondly, we assume that the time series of peak loading $Q(t)$ is a stationary random process, with no seasonal effects.[7] Both these assumptions are justified in Section 5. We want to calculate the distribution of the maximum of the mobilised anchor capacity, $Q_{mob} = Q(t)/Q_{ult}(t)$, over the design lifetime $t \in [0,T]$. In particular, we wish to calculate the failure probability $P_f := \Pr\left(\max_{t\in[0,T]} Q_{mob} > 1\right)$. To do this, we use a point process model (see e.g. Coles, 2001, Chapter 7).

Suppose that peaks of $Q(t)$ (local maxima within a moving window of ± 5 days, as described in the preceding section), which exceed the GP threshold u_{LT}, occur at times $t_1,\ldots,t_n \in [0,T]$, and denote the peaks as $P_i = Q(t_i)$. We approximate the resulting peak process by a homogeneous Poisson process with rate m (the expected number of threshold exceedances per year), and assume that the peak magnitudes P_i are independent and identically distributed, with distribution F_{GP}, and independent of the occurrence times. Define

$$M_T = \max_{t\in[0,T]} Q_{mob}(t). \tag{10}$$

The probability that $M_T \leq 1$ is equal to the probability that no peak P_i exceeds the moving boundary $Q_{ult}(t_i)$ during the interval $[0,T]$. Let N_T be the number of times the process $Q_{mob}(t)$ exceeds 1 in the interval $[0,T]$. Then we can write

$$\Pr(M_T \leq 1) = \Pr\left(N_T = 0\right). \tag{11}$$

[7] Neither of these assumptions are essential to the method, but simplify the presentation, and are reasonable for the current case study.

https://doi.org/10.5194/wes-2026-194
Preprint. Discussion started: 6 November 2026
© Author(s) 2026. CC BY 4.0 License.



eawe european academy of wind energy
Open Access WIND ENERGY SCIENCE DISCUSSIONS

N_T is a non-homogeneous Poisson process with intensity density function[8]

$$\lambda(t) = m \Pr\left(P_i > Q_{ult}(t)\right) = m\bar{F}_{GP}\big(Q_{ult}(t)\big), \tag{12}$$

where $\bar{F}_{GP}(x) = 1 - F_{GP}(x)$ is the survivor function of the GP distribution for the long-term extreme anchor load peaks. For a Poisson process (homogeneous or not), the number of events N_T occurring in an interval $[0, T]$ follows a Poisson distribution. The parameter of this distribution is the expected number of events Λ, which is the integral of the intensity over that interval:

$$\Lambda(T) = \int_0^T \lambda(t)\,\mathrm{d}t = m \int_0^T \bar{F}_{GP}\big(Q_{ult}(t)\big)\,\mathrm{d}t. \tag{13}$$

The probability that a Poisson-distributed random variable N with mean Λ is exactly k is

$$\Pr(N = k) = \frac{\Lambda^k e^{-\Lambda}}{k!}. \tag{14}$$

Therefore, the probability of anchor failure is

$$P_f = \Pr(M_T > 1) = 1 - \Pr\left(N_T = 0\right) = 1 - \exp\left(-m \int_0^T \bar{F}_{GP}\big(Q_{ult}(t)\big)\,\mathrm{d}t\right). \tag{15}$$

Here, it is assumed that $Q_{ult}(t)$ is above the GP threshold for all $t \in [0, T]$.

5 Results

5.1 Seasonality in response

The failure probability calculation described in the preceding section assumes that the peak loading on the anchor is a stationary process, with no seasonal variation. To test this assumption, we resampled a 1000-year time series of metocean conditions using the method described in Section 3.3. Random 3-hour peak loads were simulated for each time step of the resampled data. Figure 9 shows the simulated peak loads against day of year, together with conditional quantiles calculated over a 10-day moving window, for non-exceedance probabilities $0.1, 0.2, \ldots, 0.8, 0.9, 0.95, 0.99, 0.999$. Whilst there is some variation in the lower quantiles over the year, the highest quantiles are approximately stationary over the year, justifying the assumption of no seasonal variability.

5.2 Evolution of soil strength

The evolution of soil strength was found to be highly repeatable over different random sequencing of metocean conditions. Figure 10 shows the time evolution of soil damage, hardening, relative seabed strength (s_u/s_{u0}) over a 20-year period, and the hardening-strength relationship, for various combinations of anchor diameters and coefficients of consolidation, $c_v = 2.5$

[8]The intensity density function describes the expected number of points per unit time, for which $Q_{mob}(t) > 1$.

https://doi.org/10.5194/wes-2026-194
Preprint. Discussion started: 6 November 2026
© Author(s) 2026. CC BY 4.0 License.

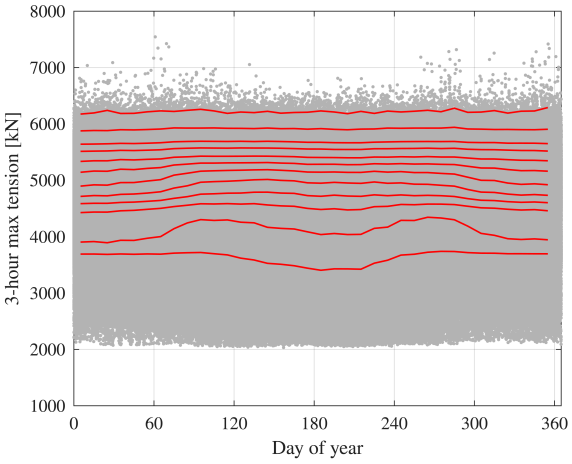


Figure 9. Dots: Random 3-hour maximum tension values from 1000 years of resampled metocean data. Lines: Conditional quantiles in 10-day moving window at non-exceedance probabilities $0.1, 0.2, \ldots, 0.8, 0.9, 0.95, 0.99, 0.999$.

and 10 m^2/year. All cases use a compression index of $\lambda_* = 0.5$. For each pair of parameter values, results are shown for ten random metocean time series. Initially, the damage is constant at $D = 1$ for all the variable combinations considered, indicating that the cyclic loading rate is large enough that pore pressure dissipation does not affect the damage level. This leads to the soil strength being reduced to the minimum level within a few weeks. However, the maximum possible rate of soil hardening occurs when $D = 1$, leading to an essentially deterministic increase in soil strength over the first 2-3 years. For the cases with the lower consolidation rate of $c_v = 2.5$ m^2/year, the damage remains constant at $D = 1$ for the 20-year lifetime. For the cases with higher consolidation rates, the soil strength increases to a level where the damage accumulation rate falls below the dissipation rate, and the damage begins to reduce. At this stage, there is a small level of variation in the damage for different random sequencing of metocean conditions. The difference in seabed strength between runs is less than 3.5%. However, as discussed below, the failure probability is dominated by the strength over the first 2 years, over which the strength is essentially deterministic, so this variability has negligible impact on the failure probability.

The reason that the damage evolution is highly repeatable is that there is relatively low variability in damage accumulation over the 28-day blocks used here. Figure 11 shows the damage accrued over 28-day blocks against the day of the year of the start of the block, for anchor diameters of 8 and 9 m. The seasonal variability in the damage accumulation is relatively weak, with only a small variation of less than 10% in the mean rate between summer and winter. Moreover, the variation in the damage accrued over a single block, starting at a given time of year is of a similar order, around 10-20%. This means that the aggregate damage over a year will have much lower variability, as observed above.

Simulations were also run using a compression index of $\lambda_* = 2.5$, although results are not shown here. The effect of increasing λ_* is to reduce the relative seabed strength s_u/s_{u0} for a given combination of H and D – see Eq. (6). This has the effect of

https://doi.org/10.5194/wes-2026-194
Preprint. Discussion started: 6 November 2026
© Author(s) 2026. CC BY 4.0 License.

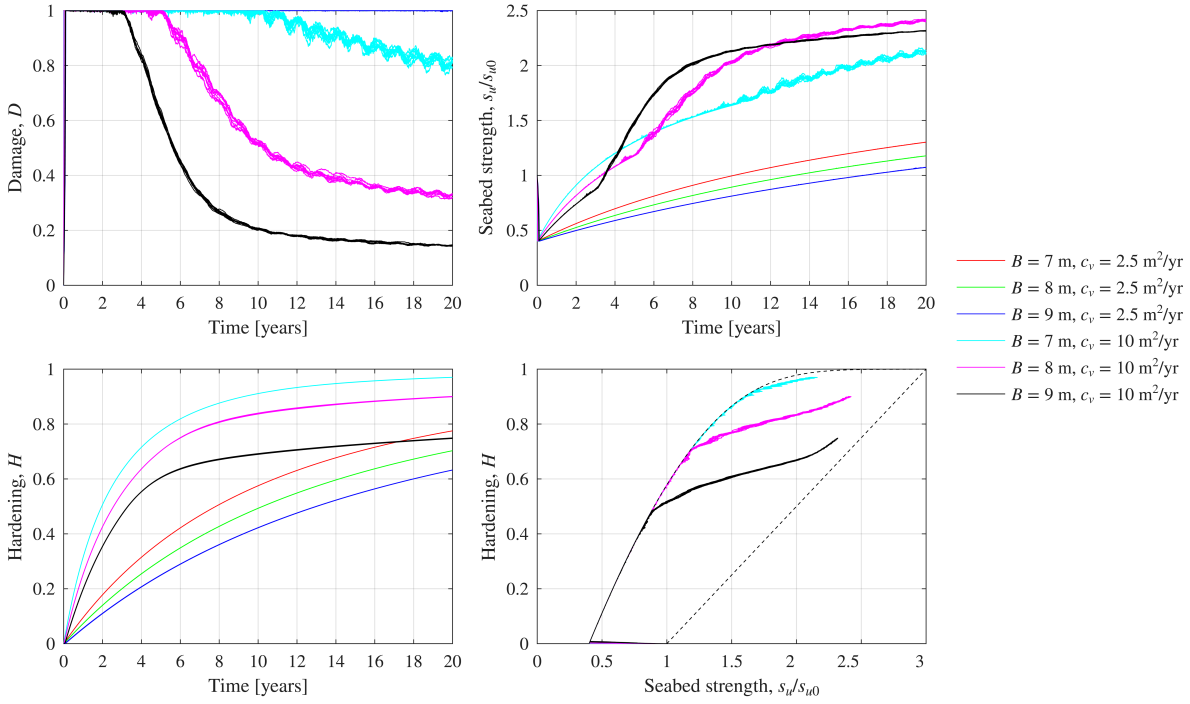


Figure 10. Evolution of soil parameters for various anchor diameters, B, and coefficients of consolidation, c_v. For each pair of parameter values, results are shown for ten random metocean time series. All cases have $\lambda_* = 0.5$.

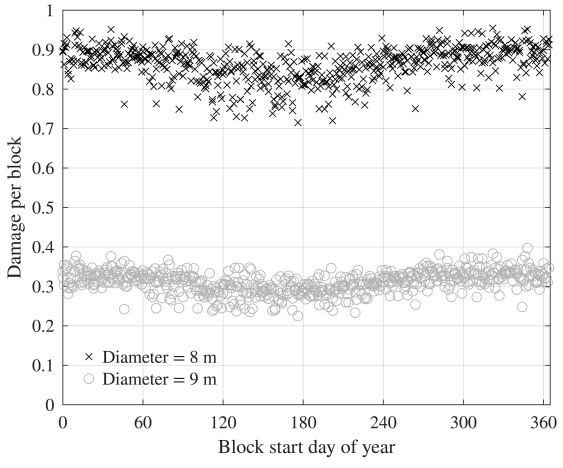


Figure 11. Damage accrued over a 28-day period against the day of the year of the start of the block. Results shown for anchor diameters of 8 and 9 m.

https://doi.org/10.5194/wes-2026-194
Preprint. Discussion started: 6 November 2026
© Author(s) 2026. CC BY 4.0 License.

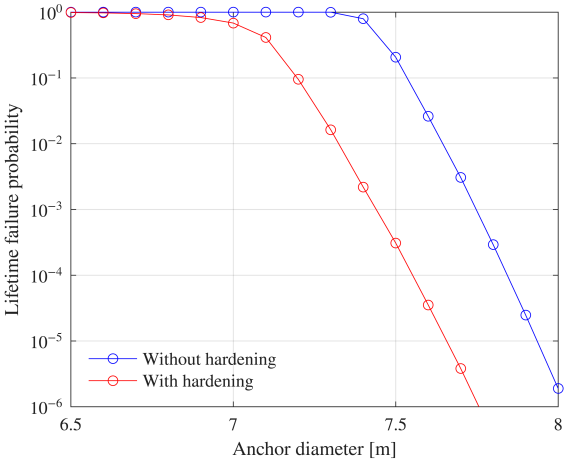


Figure 12. Lifetime failure probability as a function of anchor diameter for softening-only case and seabed hardening case with $c_v = 10$ m^2/yr.

increasing the damage accumulation rate, to the extent where it remains fixed at $D = 1$ for all combinations of c_v and anchor diameter shown in Figure 10, and the resulting seabed strength ratio s_u/s_{u0} remains less than 1 for the 20-year lifetime.

5.3 Effect of soil hardening on failure probability

To isolate the effect of soil hardening on the optimised anchor size, we use the approach outlined in Section 4 for both the cases with hardening and without hardening (where we set κ_*=0.25 or κ_*=0 respectively in Eqs (7) (8)). In the reference case, when hardening is not included in the analysis, we assume that the anchor capacity is constant and the averaged seabed undrained strength around the anchor remains at a minimum value of $s_u/s_{u0} = 1/S_{t_0}$ throughout the design lifetime. This is consistent with the DNV recommended practice for the unfactored ultimate limit state (ULS) design of a plate anchor under cyclic loading (DNV, 2021). However, in this study, we derive the applied anchor loads over the design lifetime using the surrogate model, rather than from a single worst-case storm, based on a 1 in 100-year (H_s, T_p) environmental contour, as recommended in DNV-OS-E301 (DNV, 2024). This makes the applied loading consistent with the case where seabed hardening is considered.

Figure 12 shows an example of the lifetime failure probability as a function of anchor diameter, for cases without hardening and with hardening using $c_v = 10$ m^2/year and $\lambda_* = 0.5$. As expected, when the effect of seabed hardening is considered, the anchor diameter required to achieve a given failure probability is reduced. The percentage reduction in the anchor area from accounting for seabed hardening is shown in Figure 13 as a function of lifetime failure probability. Coefficients of consolidation of $c_v = 2.5$, 5.0 and 10 m^2/yr, yield area reductions of 6-8 % (these are the 'baseline scenarios' in Figure 13).

In these cases, the minimum seabed strength ratio is $s_u/s_{u0} = 0.4$, and increases to anywhere between 1 and 2.5, depending on anchor size and consolidation rate. The relatively modest reduction of anchor area by 6-8 % from considering seabed hardening may therefore seem surprisingly low, given the larger percentage increases in seabed strength. The reason for the

https://doi.org/10.5194/wes-2026-194
Preprint. Discussion started: 6 November 2026
© Author(s) 2026. CC BY 4.0 License.

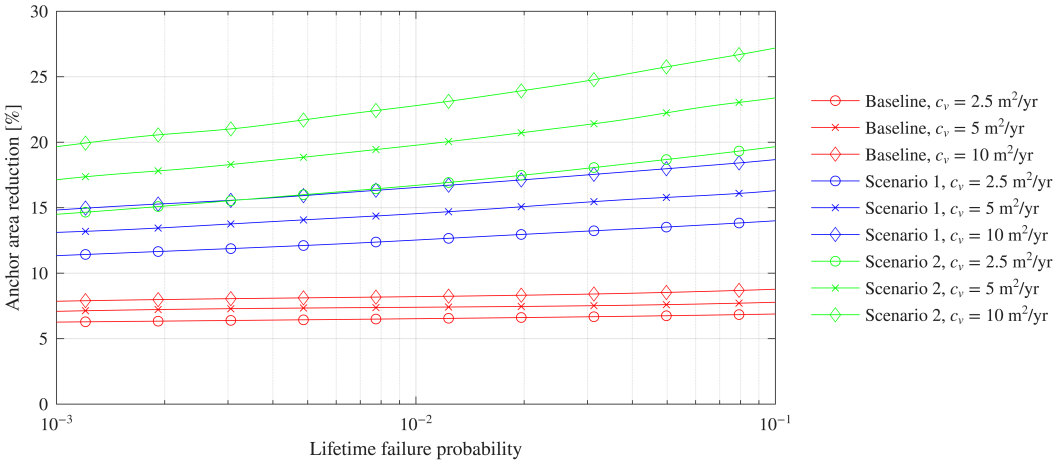


Figure 13. Reduction in anchor area required to obtain a given failure probability as a result of accounting for seabed hardening.

relatively small effect of hardening is that for the present case study parameters (turbine, platform, mooring configuration and metocean conditions), there is only a 10 % increase in the 100-year return period load, compared to the 1-year return period loads – see the baseline scenario in Figure 15. This means that large loads (relative to the 100-year return level) occur frequently, so we are likely to see a relatively large load when the soil is at its weakest point. This is because peak loads during frequently-occurring operational conditions are of a similar magnitude to peak loads occurring during storm conditions.

Figure 14 shows a time series of random 3-hour maximum mooring tension over the original metocean dataset, with points coloured according to whether the turbine is operational or idle. It is evident that relatively large loads occur frequently throughout the time series. The middle row shows the most probable 3-hour maximum load against both U_{hub} and H_s, while the bottom row shows random 3-hour maximum load against U_{hub} and H_s, using the same random values shown in the time series above. Thrust loads on the rotor around rated wind speed result in a large mean load transferred to the mooring and anchor, and similar size peak loads to those in storm conditions. For the most probable 3-hour maxima, there is a clear trend for the largest loads to occur in the largest (and rarest) sea states. However, for the random 3-hour maxima, there are similar sized loads at low H_s, corresponding to rare loads in commonly-occurring conditions.

5.4 Effect of load distribution on failure probability

At more exposed sites, with larger extreme conditions, the ratio of the 100-year to 1-year return period anchor load could be larger than in the baseline scenario considered above. Alternatively, different mooring configurations could also affect this ratio. The present case study uses a semi-taut mooring. Tension leg or catenary-moored structures could have different storm-to-operational ratios.

The failure probability in (15) is a function of (a) the long-term peak loading distribution (assumed to follow a GP distribution here); and (b) the evolution of anchor ultimate capacity, $Q_{ult}(t)$ over time. To examine sensitivity to the separation between

https://doi.org/10.5194/wes-2026-194
Preprint. Discussion started: 6 November 2026
© Author(s) 2026. CC BY 4.0 License.

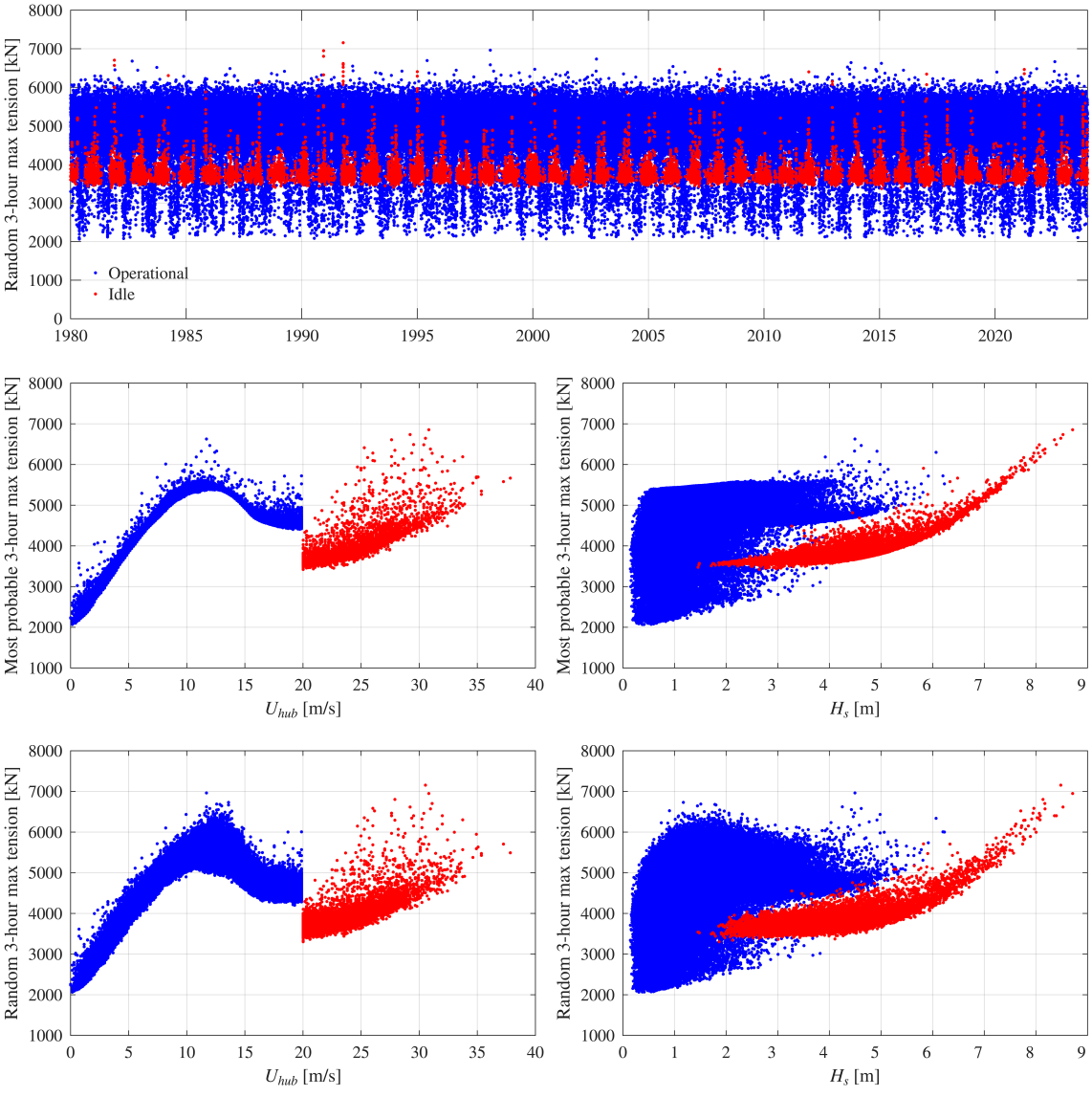


Figure 14. Illustration of how extreme loading is driven by frequently-occurring operational conditions. Top: Time series of random 3-hour maximum mooring tension over the original metocean dataset. Middle row: Most probable 3-hour maximum mooring tension against U_{hub} and H_s. Bottom row: Random 3-hour maximum mooring tension against U_{hub} and H_s (same random values shown in top row).

https://doi.org/10.5194/wes-2026-194
Preprint. Discussion started: 6 November 2026
© Author(s) 2026. CC BY 4.0 License.

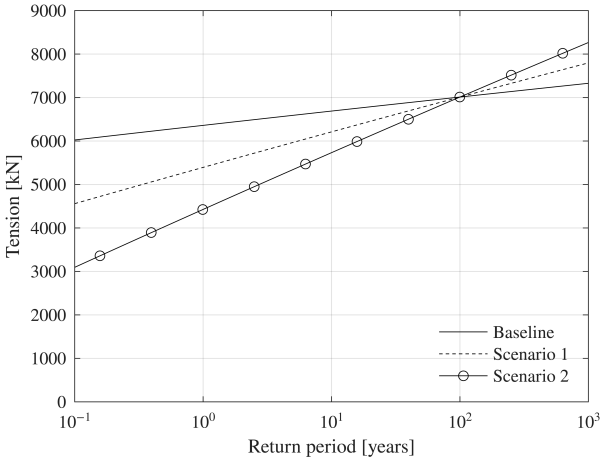


Figure 15. Baseline and alternative scenarios of mooring line tension return values.

frequent and extreme loads, we construct alternative parametric tail distributions by varying the POT threshold while retaining the same 100-year return load. We fix the 100-year return period anchor load at $x_{100} = 7011$ kN, the GP shape parameter $\xi_{LT} = -0.0087$, and the mean number of peaks per year at $m = 11.76$. These are the values estimated for the baseline scenario. We then vary the threshold and adjust the GP scale parameter to give the required 100-year return value.[9] The threshold for the baseline scenario is $u_{LT} = 6000$ kN. The threshold for scenario 1 is $u_{LT} = 4500$ kN, and for scenario 2 $u_{LT} = 3000$ kN. The corresponding scale parameters are given by $\sigma_{LT} = (x_{100} - u_{LT}) \cdot \xi_{LT} / \left((mT)^{\xi_{LT}} - 1\right)$, where $T = 100$ is the return period in years. The corresponding return values for the three scenarios are shown in Figure 15.

The reduction in the anchor area required to achieve a given failure probability for the three scenarios is shown in Figure 13. Scenarios 1 and 2, which have larger ratios of 100-year to 1-year anchor load return values, lead to larger reduction in the required anchor area. For scenario 2 and consolidation coefficient $c_v = 2.5$ m^2/year, the anchor area is reduced between 15 and 20 %, depending on the lifetime failure probability. The area reduction increases to 20-27 % for $c_v = 10$ m^2/year. So, accounting for seabed hardening leads to greater reductions in anchor size for faster consolidating seabeds and larger ratios of 100-year to 1-year anchor load return values.

5.5 Failure risk over time

Suppose that we size an anchor to support a FOWT over a typical lifetime (e.g. 20 years) and to have a failure probability of 10^{-2}. We can examine how the failure probability per year changes over time, under the different scenarios (Baseline, Scenario 1 and Scenario 2), by evaluating Equation (15) with the integral range restricted to a given time period. Figure 16 shows the failure probability per year for the three long-term load distributions considered, and three consolidation rates. In all cases, the

[9] In practice, varying the threshold will change the mean number of exceedances per year m. However, for simplicity, we hold m fixed in this sensitivity study.

https://doi.org/10.5194/wes-2026-194
Preprint. Discussion started: 6 November 2026
© Author(s) 2026. CC BY 4.0 License.

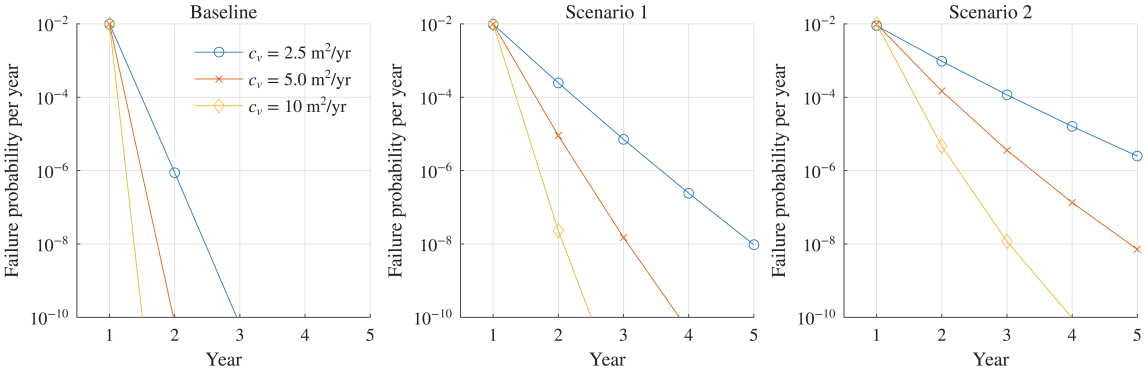


Figure 16. Failure probability per year for an anchor sized to have a 20-year lifetime failure probability of 10^{-2}. The three plots correspond to the three long-term load distributions. Results shown for consolidation rates of $c_v = 2.5$, 5.0 and 10 m^2/year.

failure risk is dominated by the risk in the first year, when the soil is at its weakest point. For the baseline load distribution, the failure risk in year two is less than 10^{-6} for $c_v = 2.5$ m^2/year and 10^{-17} for $c_v = 10$ m^2/year. The risk decreases more quickly for the faster consolidation rate, as the seabed strength and hence anchor capacity increases faster, meaning that the risk of a load exceeding the capacity decreases rapidly. For scenario 2, which has the largest ratio of 100-year to 1-year return values, the failure risk decreases at a slower rate, since the likelihood of a large load occurring in the first year is reduced. Nevertheless, the lifetime failure risk is still dominated by the year 1 failure risk, with the failure risk in year two being at least an order of magnitude lower.

The failure in each year also changes based on the anchor size. Figure 17 shows the failure probability per year for anchors with diameters ranging from 6 m (blue lines) to 8 m (yellow lines) at increments of 0.1 m, for $c_v = 2.5$ m^2/year. Visualisation of the results in this format can be helpful to inform anchor design, particularly the required anchor size for different failure probabilities per year. For the baseline case, anchors with a diameter less than 7.1 m are effectively guaranteed to fail in the first year (failure probability in excess of 0.99999). Anchors with diameters greater than 7.4 m are required to achieve a failure probability less than 10^{-2} in the first year. For these larger anchors, the probabilities of failure decrease rapidly in subsequent years, as also shown in Figure 16. The same minimum anchor diameter of 7.4 m is required to achieve a failure probability of less than 10^{-2} in the first year for scenarios 1 and 2. However, the rate of reduction of the failure probabilities per year in scenarios 1 and 2 is less than in the baseline case for all anchor sizes. This highlights how whole-life anchor response is linked to the loads transmitted to the anchoring system, and these are dependent on the site conditions and response of the floating offshore wind turbine.

6 Conclusions

A probabilistic design framework has been presented for assessing the lifetime failure risk and design of deeply embedded plate anchors for floating and other deepwater offshore wind applications. The framework combines probabilistic simulation of

https://doi.org/10.5194/wes-2026-194
Preprint. Discussion started: 6 November 2026
© Author(s) 2026. CC BY 4.0 License.

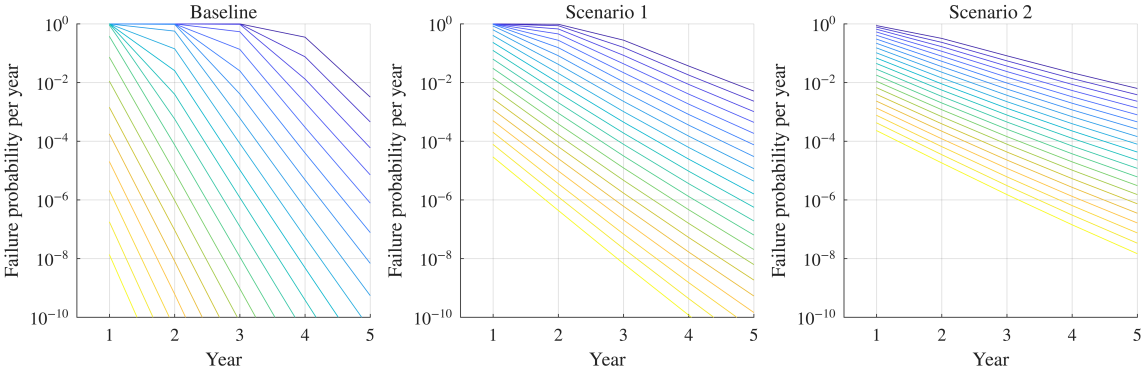


Figure 17. Failure probability per year for anchors with diameter 6 m (blue lines) to 8 m (yellow lines) at increments of 0.1 m. Results are shown for a consolidation rate of $c_v = 2.5$ m^2/year. The three plots correspond to the three long-term load distributions.

lifetime anchor loading with whole-life geotechnical modelling of seabed damage accumulation, pore-pressure dissipation and consolidation-induced hardening. A probabilistic surrogate model provides an efficient means of generating stochastic anchor load histories from metocean conditions, while block resampling provides synthetic lifetime metocean sequences that retain the observed multivariate distribution, short-term temporal structure and seasonal variability. Extreme anchor loads beyond the range of the resampled metocean data are accounted for using peaks-over-threshold extrapolation, allowing the time-varying anchor capacity to be incorporated into a probabilistic failure calculation.

The framework was demonstrated for a 15 MW floating offshore wind turbine at a site in the Scottish North Sea. The results show that cyclic loading initially drives the seabed to a reduced-strength state, followed by recovery as consolidation occurs. The strength evolution was found to be highly repeatable between different random realisations of the metocean conditions, with differences in seabed strength of less than 3.5% between realisations in the cases considered. For the baseline load distribution, accounting for seabed hardening reduced the anchor area required to achieve a given lifetime failure probability by approximately 6–8%.

The results also demonstrate that the benefit of whole-life geotechnical modelling depends strongly on the distribution of anchor loads. In the baseline case, the 100-year return-period load is only approximately 10% greater than the 1-year return-period load. Consequently, relatively large loads occur sufficiently frequently that there is a substantial probability of experiencing high loading while the seabed is still close to its minimum-strength state, limiting the reduction in required anchor area obtained from consolidation. When alternative load distributions are considered with greater separation between frequently occurring and extreme loads, the potential reduction in required anchor area increases substantially, reaching up to 27% in the cases examined.

These results indicate that the value of whole-life geotechnical design cannot be characterised solely by the magnitude of seabed strength recovery. Instead, its impact on anchor design depends on the interaction between the evolution of anchor capacity and the statistical distribution of loads transmitted by the complete offshore renewable energy system. In particular,

https://doi.org/10.5194/wes-2026-194
Preprint. Discussion started: 6 November 2026
© Author(s) 2026. CC BY 4.0 License.



systems for which extreme loads are of a similar magnitude to operational loads may obtain less benefit from seabed hardening than systems with a greater separation between routine and extreme loading. The design implications of whole-life geotechnical modelling are therefore expected to depend on both site conditions and the dynamic response of the turbine, floater and mooring system.

For the present case study, failure risk is concentrated in the early part of the operational lifetime, when seabed strength is at its lowest. The calculated annual failure probability decreases substantially after the first year as consolidation increases anchor capacity, particularly for faster-consolidating seabeds. This highlights the potential importance of considering the temporal evolution of both loading and capacity rather than basing anchor design solely on a constant minimum seabed strength.

The framework presented here provides a basis for extending probabilistic whole-life anchor design to different site conditions, turbine and mooring configurations, and offshore renewable energy systems. Future work could incorporate uncertainty in seabed properties and mooring response, directional and environmental variability, and the coupling between anchor response and the mooring–seabed interaction.

Code and data availability. Data and code will be made available upon request.

Author contributions. **Ed Mackay**: Conceptualization, Methodology, Software, Validation, Visualization, Formal Analysis, Investigation, Writing - original draft, Funding acquisition. **Ajit Pillai**: Conceptualization, Methodology, Software, Validation, Formal Analysis, Investigation, Resources, Writing - Review & Editing, Funding acquisition. **Katherine Kwa**: Conceptualisation, Methodology, Validation, Writing - Review & Editing, Funding acquisition.

Competing interests. The authors declare they have no competing interests.

Acknowledgements. This work was funded by the EPSRC Supergen Offshore Renewable Energy Hub, United Kingdom [grant no: EP/Y016297/1] under the NextGen Anchor flexible fund project. A. C. Pillai and K.A Kwa acknowledge support from the Royal Academy of Engineering under the Research Fellowship scheme [Awards RF\202021\20\175 and RF 2122-21-119]. The metocean data was supplied by the UK Met Office.

https://doi.org/10.5194/wes-2026-194
Preprint. Discussion started: 6 November 2026
© Author(s) 2026. CC BY 4.0 License.



eawe european academy of wind energy
Open Access WIND ENERGY SCIENCE DISCUSSIONS

References

Allen, C., Viscelli, A., Dagher, H., Goupee, A., Gaertner, E., Abbas, N., Hall, M., and Barter, G.: Definition of the UMaine VolturnUS-S reference platform developed for the IEA wind 15-Megawatt offshore reference wind turbine, Tech. Rep. NREL/TP-5000-76773, National Renewable Energy Lab.(NREL), Golden, CO (United States), https://docs.nlr.gov/docs/fy20osti/76773.pdf, 2020.

Andersen, K. and Lauritzen, R.: Cyclic bearing capacity analysis for gravity platforms; calculation procedure, verification by model tests, and application for the Gullfaks C platform, in: Procs. of Intl. Conference on Behaviour of Offshore Structures (BOSS '88), vol. 1, pp. 311–324, Trondheim, Norway, https://www.issmge.org/filemanager/technical_committees/20/The-Third-McClelland-Lecture-Knut-H-Andersen-presentation.pdf, 1988.

Andersen, K. H. et al.: Cyclic soil parameters for offshore foundation design, Frontiers in offshore geotechnics III, 5, 2015.

ASTM International: Standard Practices for Cycle Counting in Fatigue Analysis, ASTM E1049-85, https://store.astm.org/e1049-85r17.html, 2023.

Bai, Y., Yan, H.-b., Cao, Y., Kim, Y., Yang, Y.-y., and Jiang, H.: Time-dependent reliability assessment of offshore jacket platforms, Ships and Offshore Structures, 11, 591–602, https://doi.org/10.1080/17445302.2015.1038869, 2016.

Bonjean, D., Erbrich, C., and Zhang, G.: Pipeline Floatation Assessment in Liquefiable Soil, in: Offshore Technology Conference, pp. OTC–19 668, OTC, https://doi.org/10.4043/19668-MS, 2008.

Cai, Y., Bransby, M. F., Gaudin, C., and Tian, Y.: Accounting for soil spatial variability in plate anchor design, Journal of Geotechnical and Geoenvironmental Engineering, 148, 04021 178, https://doi.org/10.1061/(ASCE)GT.1943-5606.0002720, 2022.

Cerfontaine, B., White, D., Kwa, K., Gourvenec, S., Knappett, J., and Brown, M.: Anchor geotechnics for floating offshore wind: Current technologies and future innovations, Ocean Engineering, 279, 114 327, https://doi.org/10.1016/j.oceaneng.2023.114327, 2023.

Clarindo, G., Vanem, E., and Soares, C. G.: Modelling multivariate serially correlated sea states, Ocean Engineering, 361, 126 106, https://doi.org/10.1016/j.oceaneng.2026.126106, 2026.

Cocjin, M., Gourvenec, S., White, D., and Randolph, M.: Tolerably mobile subsea foundations–observations of performance, Géotechnique, 64, 895–909, https://doi.org/10.1680/geot.14.P.098, 2014.

Cocjin, M. L., Gourvenec, S. M., White, D. J., and Randolph, M. F.: Theoretical framework for predicting the response of tolerably mobile subsea installations, Géotechnique, 67, 608–620, https://doi.org/10.1680/jgeot.16.P.137, 2017.

Coles, S.: An Introduction to Statistical Modeling of Extreme Values, Springer, 2001.

DNV: Design and installation of plate anchors in clay, Recommended Practice DNV-RP-E302, https://www.dnv.com/energy/standards-guidelines/dnv-rp-e302-design-and-installation-of-plate-anchors-in-clay/, 2021.

DNV: Position mooring, Offshore Standard DNV-OS-E301, 2024.

Gaertner, E., Rinker, J., Sethuraman, L., Zahle, F., Anderson, B., Barter, G., Abbas, N., Meng, F., Bortolotti, P., Skrzypinski, W., Scott, G., Feil, R., Bredmose, H., Dykes, K., Shields, M., Allen, C., and Viselli, A.: Definition of the IEA 15-Megawatt Offshore Reference Wind Turbine, Tech. Rep. NREL/TP-5000-75698, National Renewable Energy Lab.(NREL), Golden, CO (United States), https://docs.nlr.gov/docs/fy20osti/75698.pdf, 2020.

Gourvenec, S.: Whole-life geotechnical design: What is it? What's it for? So what? And what next?, in: Proceedings 4th International Symposium on Frontiers in Offshore Geotechnics, Deep Foundations Institute, https://eprints.soton.ac.uk/id/eprint/449462/, 2020.

Gourvenec, S.: Whole life design: Theory and applications of this new approach to offshore geotechnics, Indian Geotechnical Journal, 52, 1129–1154, https://doi.org/10.1007/s40098-022-00627-x, 2022.

https://doi.org/10.5194/wes-2026-194
Preprint. Discussion started: 6 November 2026
© Author(s) 2026. CC BY 4.0 License.

Han, C., Wang, D., Gaudin, C., O'Loughlin, C., and Cassidy, M.: Behaviour of vertically loaded plate anchors under sustained uplift, Géotechnique, 66, 681–693, https://doi.org/10.1680/jgeot.15.P.232, 2016.

Hodder, M., White, D., and Cassidy, M.: An effective stress framework for the variation in penetration resistance due to episodes of remoulding and reconsolidation, Géotechnique, 63, 30–43, https://doi.org/10.1680/geot.9.P.145, 2013.

IEC: Wind energy generation systems - Part 1: Design requirements, International Electrotechnical Commission, Standard IEC 61400-3-1, https://webstore.iec.ch/en/publication/29360, 2019.

Jiang, P., Zhou, Q., and Shao, X.: Surrogate model-based engineering design and optimization, Springer, 2020.

Künsch, H. R.: The jackknife and the bootstrap for general stationary observations, The Annals of Statistics, pp. 1217–1241, https://doi.org/10.1214/aos/1176347265, 1989.

Kwa, K., White, D., Tosdevin, T., Jin, S., and Greaves, D.: Whole-life modelling of anchor capacity for floating systems: The RSN-CSI approach, Applied Ocean Research, 138, 103 671, https://doi.org/10.1016/j.apor.2023.103671, 2023a.

Kwa, K. A., Festa, O., White, D. J., Gourvenec, S., and Sobey, A.: Design benefits for plate anchors for floating offshore wind through coupling floater, mooring and geotechnical responses, SUT Offshore Site Investigation and Geotechnics, pp. SUT–OSIG–23–135, https://doi.org/10.3723/XTOM8787, 2023b.

Laham, N., Kwa, K., White, D., and Gourvenec, S.: Episodic simple shear tests to measure strength changes for whole-life geotechnical design, Géotechnique Letters, 11, 103–111, https://doi.org/10.1680/jgele.20.00124, 2021.

Laham, N., Kwa, K., Suzuki, Y., White, D., and Gourvenec, S.: Effect of episodic pre-failure cyclic loading on whole-life geotechnical properties of soft clays, Géotechnique, 75, 225–236, https://doi.org/10.1680/jgeot.24.00063, 2025a.

Laham, N., Kwa, K., White, D., and Gourvenec, S.: A surrogate model to efficiently predict changing strength and stiffness of soft soils through whole-life episodic cyclic loading, Computers and Geotechnics, 177, 106 895, https://doi.org/10.1016/j.compgeo.2024.106895, 2025b.

Lai, Y., Wang, L., Hong, Y., and He, B.: Centrifuge modeling of the cyclic lateral behavior of large-diameter monopiles in soft clay: Effects of episodic cycling and reconsolidation, Ocean Engineering, 200, 107 048, https://doi.org/10.1016/j.oceaneng.2020.107048, 2020.

Mackay, E. and Johanning, L.: A simple and robust method for calculating return periods of ocean waves, in: International Conference on Offshore Mechanics and Arctic Engineering, vol. 51333, p. V11BT12A060, American Society of Mechanical Engineers, https://doi.org/10.1115/OMAE2018-78729, 2018a.

Mackay, E. and Johanning, L.: Long-term distributions of individual wave and crest heights, Ocean Engineering, 165, 164–183, https://doi.org/10.1016/j.oceaneng.2018.07.047, 2018b.

Mackay, E., de Hauteclocque, G., Vanem, E., and Jonathan, P.: The effect of serial correlation in environmental conditions on estimates of extreme events, Ocean Engineering, 242, 110 092, https://doi.org/10.1016/j.oceaneng.2021.110092, 2021.

Mackay, E., Pillai, A., and Kwa, K.: Development of a Probabilistic Surrogate Model for Loads on an Embedded Plate Anchor. Part I: Short-term Extreme Loads, in: International Conference on Offshore Mechanics and Arctic Engineering, pp. OMAE2026–175 098, https://doi.org/10.1115/OMAE2026-175098, 2026a.

Mackay, E., Pillai, A., and Kwa, K.: Development of a Probabilistic Surrogate Model for Loads on an Embedded Plate Anchor. Part II: Cyclic Loads, in: International Conference on Offshore Mechanics and Arctic Engineering, pp. OMAE2026–181 827, https://doi.org/https://doi.org/10.1115/OMAE2026-181827, 2026b.

Marine Scotland: National Marine Plan Interactive Map, https://marinescotland.atkinsgeospatial.com/nmpi/default.aspx?layers=745, accessed: 2026-06-16, 2013.

https://doi.org/10.5194/wes-2026-194
Preprint. Discussion started: 6 November 2026
© Author(s) 2026. CC BY 4.0 License.

Martin, C. and Randolph, M.: Applications of the lower and upper bound theorems of plasticity to collapse of circular foundations, in: Proc., 10th Int. Conf. on Computer Methods and Advances in Geomechanics, vol. 2, pp. 1417–1428, 2001.

Mentani, A., Govoni, L., Gaudin, C., Watson, P., and Tian, Y.: Predicting the uniaxial capacity of plate anchors in spatially variable clay using metamodels, Computers and Geotechnics, 182, 107 157, https://doi.org/10.1016/j.compgeo.2025.107157, 2025.

O'Loughlin, C. D., Zhou, Z., Stanier, S., and White, D.: Load-controlled cyclic T-bar tests: a new method to assess effects of cyclic loading and consolidation, Géotechnique letters, 10, 7–15, https://doi.org/10.1680/jgele.19.00030, 2020.

Orcina Ltd: K03 Renewables: 15MW semi-sub FOWT, https://www.orcina.com/wp-content/uploads/examples/k/k03/K03%2015MW%20semi-sub%20FOWT.pdf, 2025.

Politis, D. N. and Romano, J. P.: The stationary bootstrap, Journal of the American Statistical association, 89, 1303–1313, https://doi.org/10.1080/01621459.1994.10476870, 1994.

Randolph, M. and Gourvenec, S.: Offshore geotechnical engineering, CRC press, 2017.

Rui, S., Zhou, Z., Gao, Z., Jostad, H. P., Wang, L., Xu, H., and Guo, Z.: A review on mooring lines and anchors of floating marine structures, Renewable and Sustainable Energy Reviews, 199, 114 547, https://doi.org/10.1016/j.rser.2024.114547, 2024.

Rui, S., Jostad, H. P., Zhou, Z., Bachynski-Polić, E., Sævik, S., Wang, L., and Guo, Z.: Analysis of mooring system for floating wind turbine based on macro-model of chain-seabed interaction, Marine Structures, 104, 103 877, https://doi.org/10.1016/j.marstruc.2025.103877, 2025.

Samadian, D., Muhit, I. B., and Dawood, N.: Application of data-driven surrogate models in structural engineering: a literature review, Archives of Computational Methods in Engineering, 32, 735–784, https://doi.org/10.1007/s11831-024-10152-0, 2025.

Smith, V. and White, D.: Volumetric hardening in axial pipe soil interaction, in: Offshore Technology Conference Asia, pp. OTC–24 856, OTC, https://doi.org/https://doi.org/10.4043/24856-MS, 2014.

Solari, S., Egüen, M., Polo, M. J., and Losada, M. A.: Peaks Over Threshold (POT): A methodology for automatic threshold estimation using goodness of fit p-value, Water Resources Research, 53, 2833–2849, https://doi.org/10.1002/2016WR019426, 2017.

Stanier, S. and White, D.: Enhancement of bearing capacity from consolidation: due to changing strength or failure mechanism?, Géotechnique, 69, 166–173, https://doi.org/10.1680/jgeot.17.T.030, 2019.

Tendijck, S., Jonathan, P., Randell, D., and Tawn, J.: Temporal evolution of the extreme excursions of multivariate kth order Markov processes with application to oceanographic data, Environmetrics, 35, e2834, https://doi.org/10.1002/env.2834, 2024.

Tom, J. G., Rijnsdorp, D. P., Ragni, R., and White, D. J.: Fluid-structure-soil interaction of a moored wave energy device, in: International Conference on Offshore Mechanics and Arctic Engineering, vol. 58899, p. V010T09A024, American Society of Mechanical Engineers, https://doi.org/https://doi.org/10.1115/OMAE2019-95419, 2019.

UK Met Office: Atlantic- European North West Shelf- Wave Physics Reanalysis, https://doi.org/10.48670/moi-00060, 2025.

Verruijt, A.: Computational geomechanics, vol. 7, Springer Science & Business Media, 1995.

Wang, C., O'Loughlin, C. D., Bransby, M., Watson, P., and Zhou, Z.: Consolidation-induced improvements in plate anchor capacity, Canadian Geotechnical Journal, 60, 1264–1275, https://doi.org/10.1139/cgj-2022-0382, 2023.

White, D., Doherty, J., Guevara, M., and Watson, P.: A cyclic py model for the whole-life response of piles in soft clay, Computers and Geotechnics, 141, 104 519, https://doi.org/10.1016/j.compgeo.2021.104519, 2022.

Zhang, W., Zhou, Z., Pradhan, D. L., Wang, P., and Jin, H.: Design considerations of drag anchors in cohesive soil for floating facilities in the South China sea, Marine Structures, 81, 103 101, https://doi.org/10.1016/j.marstruc.2021.103101, 2022.

https://doi.org/10.5194/wes-2026-194
Preprint. Discussion started: 6 November 2026
© Author(s) 2026. CC BY 4.0 License.



eawe european academy of wind energy
Open Access WIND ENERGY SCIENCE DISCUSSIONS

Zhou, Z., O'Loughlin, C. D., White, D. J., and Stanier, S. A.: Improvements in plate anchor capacity due to cyclic and maintained loads combined with consolidation, Géotechnique, 70, 732–749, https://doi.org/10.1680/jgeot.19.TI.028, 2020.